


# Highly Confined Surface Plasmon Polaritons from Graphene Quantum Cherenkov Effect

Chengpeng Yu<sup>1,2</sup> and Shenggang Liu<sup>1,2,\*</sup>

<sup>1</sup>Terahertz Science and Technology Research Center, University of Electronic Science and Technology of China, Chengdu, Sichuan 610054, China

<sup>2</sup>Cooperative Innovation Center of Terahertz Science, University of Electronic Science and Technology of China, Chengdu, Sichuan 610054, China

 (Received 5 June 2019; revised manuscript received 14 October 2019; published 7 November 2019)

A method for the effective excitation of Highly Confined Surface Plasmon Polaritons (HC SPPs) that can generate x-rays is presented based on the electron beam excitation of hot carriers and the graphene hot carrier quantum Cherenkov effect. Compared with the widely used methods of HC SPPs' excitation, in this method, no periodic structure is needed, so it is possible to achieve a miniaturized system; it can also excite monochromatic HC SPPs with a guide wavelength as small as 1/300 of the vacuum wavelength. The working point of HC SPPs is not sensitive to the velocity of the electron beam and can be dynamically tuned through the Fermi energy of graphene. At the same time, the working efficiency can be significantly improved (to about 37.28%). Based on the above-mentioned characteristics, when the HC SPPs and the electron beam in this method are used in the electron-plasmon scattering system, x-ray emission can be achieved with rather low electron beam energy (35 KeV). Since the electron beam can simultaneously act as the SPPs' source and the scatterer, it is possible to integrate an x-ray source and the HC SPPs' emitter that drives the x-ray source in the same cavity, realizing a unified system.

DOI: [10.1103/PhysRevApplied.12.054018](https://doi.org/10.1103/PhysRevApplied.12.054018)

## I. INTRODUCTION

Surface Plasmon Polaritons (SPPs) are collective oscillations of charged particles that propagate along the surface of plasmonic materials [1].

Highly Confined SPPs (HC SPPs) are SPPs with an electromagnetic field attenuating extremely rapidly away from both sides of the surface of the plasmonic materials. The guide wavelength along the surface (or the in-plane wavelength) is particularly short and the phase velocity is particularly low [2]. In the following part of the paper, the guide wavelength along the surface will be simply called the guide wavelength. The guide wavevector along the surface will be simply called the guide wavevector. The length of the guide wavevector will be simply called the guide wave number.

HC SPPs strengthen the light-matter interaction and compress the size of relevant systems, which is very important to electron-plasmon scattering [3,4], the excitation of quantum emitters [2,5–7], the miniaturization of optical devices [8–10], and so on.

However, the excitation of HC SPPs is not a simple problem [9,11–13]. First, optical coupling cannot effectively excite HC SPPs because there is a large mismatch

between the guide wavelength of HC SPPs and the wavelength of free space photons. Second, the near-field coupling of charged particles cannot effectively excite HC SPPs because the phase velocity of HC SPPs is significantly lower than the velocity of charged particles moving in vacuum. In addition, HC SPPs tend to have non-negligible losses [8,9,14], which require high excitation strength.

For example, in order to obtain x-rays from electron-plasmon scattering [3,4], the guide wavelength of SPPs is required to be 1/180 of the vacuum wavelength, corresponding to a phase velocity of 0.0056c (where c is the speed of light in vacuum). Either by a traditional optical or an electronic approach, the HC SPPs cannot be excited very efficiently (e.g., to obtain such SPPs, a laser pulse with a field strength of 0.1 GV/m and a metamaterial with a period of 85 nm has to be introduced [4]). If we can propose a method that excites these HC SPPs more effectively, and even HC SPPs with a higher degree of confinement, we can significantly improve the performance of the relevant systems and relax the requirements for parameters such as the energy of the electron beam that is involved in scattering (5 GeV).

A promising approach to achieve this goal is to make further use of the interaction between charged particles and media. There are many famous phenomena that belongs

\*liusg@uestc.edu.cn

to this category, for example, Cherenkov radiation [15], transient radiation [16], and Askaryan radiation (coherent radio Cherenkov pulses from particle showers in dense dielectric media) [17,18].

Among a wide variety of media, graphene is a particularly suitable one. Many works have shown that graphene is capable of sustaining HC SPPs with relatively low loss [11,19–22]. In addition, graphene also exhibits many nontrivial properties when interacting with an electron beam, which often leads to the emission of electromagnetic energy [23–25]. One very interesting example is the work of Tao *et al.* [26], which studied the emission of SPPs on graphene by the Cherenkov effect of an electron beam. However, the degree of confinement of the emitted SPPs is still limited, so the emitted SPPs cannot be used in many applications (for example, the x-ray emission discussed above).

To excite HC SPPs, we notice that in graphene, there are coupling mechanisms between hot carriers (Dirac fermions whose kinetic energy and effective temperature are higher than the average level in the material [27]) and SPPs [28–30]. Among these coupling mechanisms, the Hot Carrier Quantum Cherenkov Effect (HC QCE) is a two-dimensional version of ordinary Cherenkov radiation [31]. When the velocity of the hot carriers exceeds the phase velocity of the SPPs, it allows the excitation of a shock-wave of SPPs in the direction given by the Cherenkov angle. The working efficiency of HC QCE can reach as high as 78% [28].

Since the velocity of hot carriers is usually significantly lower than the velocity of free space charged particles, SPPs with very low phase velocity can be excited by HC QCE. In addition, the efficiency of HC QCE is relatively high. Thus, HC QCE is an effective way to solve the excitation problem of HC SPPs. However, in order to realize the vision of the excitation of HC SPPs with HC QCE, three issues have to be addressed:

(a) The frequency spectrum of SPPs excited by HC QCE is quite complex. There are multiple broadband peaks. Only some of them correspond to HC SPPs [28]. However, monochromatic HC SPPs are required in many applications [3,4,32–34].

(b) HC QCE puts a special requirement on the hot carriers that act as the source [28]. We do not find any detailed study on the possible hot carrier excitation mechanisms for HC QCE [35–37].

(c) HC QCE is possible both in positively ( $E_F > 0$ ) and negatively ( $E_F < 0$ ) doped graphene. However, we did not find any detailed study on the positively doped situation [28]. On the other hand, SPPs in a positively doped situation are needed for many applications [38–41].

In this work, we theoretically propose a method to introduce an electron beam as the source of hot carriers, thus

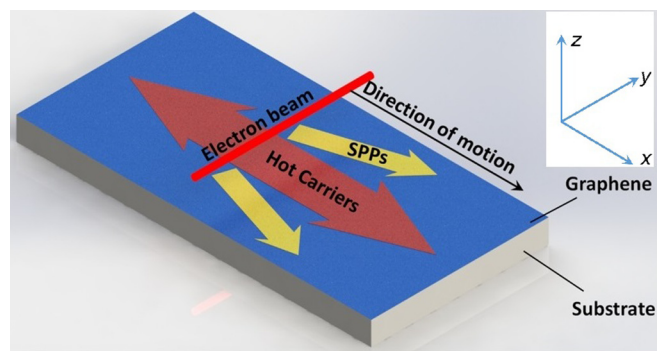


FIG. 1. The system to excite HC SPPs. A graphene monolayer is on a dielectric substrate of permittivity  $\epsilon_s = 2.1$  polymethylpentene (TPX). An electron beam of velocity  $u_0$  moves uniformly along the  $x$  direction. The graphene monolayer locates at  $z = 0$  and the distance between the electron beam and graphene monolayer is  $z_0 = 20$  nm. The electron beam excites hot carriers in the graphene. The hot carriers then emit SPPs based on HC QCE. The inset shows the coordinate system.

settling the above-mentioned issues, and then monochromatic HC SPPs can be excited. The system consists of a graphene monolayer on a dielectric substrate and an electron beam moving uniformly along it, as shown in Fig. 1.

Figure 1 shows that compared with the widely used methods of HC SPPs' excitation [8,9,12], in this method no periodic structure is not needed, so it is possible to achieve a miniaturized system.

In the following part of this paper, we will show that: (a) Based on this method, monochromatic HC SPPs can be excited. The guide wavelength of the excited HC SPPs is as small as 1/300 of the vacuum wavelength. (b) The working point of the HC SPPs (i.e., the guide wavelength and the frequency) can be dynamically tuned through the Fermi energy of graphene. At the same time, it is not sensitive to the velocity of the electron beam, so there is a wide range of choices for the velocity of the electron beam. (c) The working efficiency of the method is relatively high, up to 37.28% as estimated. (d) When the HC SPPs and the electron beam in this method are used in the electron-plasmon scattering system [3], x-ray emission can be achieved with rather low electron beam energy (35 KeV). Since the electron beam can simultaneously act as the SPPs' source and the scatterer, it is possible to integrate an x-ray source and the HC SPPs' emitter that drives the x-ray source in the same cavity, realizing a unified system.

## II. EXCITATION MECHANISM

In the system of this method, the excitation of HC SPPs consists of two steps:

(a) The electron beam excitation of hot carriers. When the electron beam moves above graphene, the Dirac

fermions in graphene are affected by the near field of the electron beam. Mediated by the field, the Dirac fermions are able to exchange photons with the electron beam. Then the Dirac fermions are excited as hot carriers. Near the Dirac point, the effective mass of the Dirac fermions is zero, and the velocity of the Dirac fermions (which is equal to the Fermi velocity  $v_F = c/300$ ) is much smaller than the velocity of the electron beam  $u_0$  [42]. Therefore, the momentum of the electron beam is much larger than that of the Dirac fermions. This means that the excited hot carriers are likely to have a narrow distribution in the momentum space, which is particularly beneficial for our purpose of exciting monochromatic HC SPPs.

It is worth noting that graphene is more suitable for the requirements of the system than other materials (Ni, etc.). Although electron beam excitation of hot carriers is also possible in other materials [43], in general, the hot carrier life is significantly shorter than in graphene [22,44,45]. The narrow momentum distribution of hot carriers is quickly smoothed out.

In addition to hot carriers, the electron beam also excites SPPs directly on graphene by means of near-field coupling. However, the guide wavelength of these SPPs is  $\lambda = u_0/f$ . This wavelength is much longer than that of our interested HC SPPs, indicating that these SPPs are not highly confined [1,46,47]. Therefore, these SPPs are not in the wavelength range discussed in this paper.

(b) HC QCE. Once the hot carriers are excited, they move on the graphene with constant velocity  $v_F$  [42]. Based on HC QCE, the hot carriers are able to excite SPPs with a phase velocity satisfying  $v_p < v_F$ , corresponding to SPPs' guide wavelength being smaller than  $1/300$  of the vacuum wavelength. Thus, the excited SPPs are highly confined as we expected. In addition, the excited SPPs' modes will also concentrate near a single working point due to the narrow distribution of hot carriers on the momentum space.

### III. THEORETICAL MODEL

To describe the above-mentioned excitation mechanism, a theoretical study is presented as below.

#### A. Quantum description of the Dirac fermions and SPPs in graphene

HC QCE is a quantum phenomenon [28], therefore, it is necessary to describe the Dirac fermions and SPPs in graphene by means of the quantum theory.

Based on the famous massless Dirac-like Hamiltonian, in a Dirac cone  $K$  ( $K'$ ), the wave functions of Dirac fermions satisfy:  $-i\hbar v_F \boldsymbol{\sigma} \cdot \nabla \psi^K = i\hbar(\partial/\partial t)\psi^K$  and  $-i\hbar v_F \boldsymbol{\sigma}^* \cdot \nabla \psi^{K'} = i\hbar(\partial/\partial t)\psi^{K'}$ , respectively, where  $\psi^K$  ( $\psi^{K'}$ ) are the two-component wave function of Dirac fermions in a Dirac cone  $K$  ( $K'$ );  $\boldsymbol{\sigma}$  are the Pauli matrices [42]. Thus, the wave functions of Dirac fermions with

momentum  $\mathbf{p}$  are

$$\psi^K(\mathbf{r}, t; \mathbf{p}, s) = \frac{1}{\sqrt{2S}} \begin{bmatrix} 1 \\ se^{i\theta} \end{bmatrix} e^{i(\mathbf{p}\cdot\mathbf{r}/\hbar)} e^{-is(v_F p/\hbar)t}, \quad (1)$$

$$\psi^{K'}(\mathbf{r}, t; \mathbf{p}, s) = \frac{1}{\sqrt{2S}} \begin{bmatrix} 1 \\ se^{-i\theta} \end{bmatrix} e^{i(\mathbf{p}\cdot\mathbf{r}/\hbar)} e^{-is(v_F p/\hbar)t}, \quad (2)$$

where  $S$  is the area of graphene, the pseudo spin  $s = \pm 1$  labels whether the Dirac fermions belong to the upper or lower half of a Dirac cone, and  $\theta$  is the angle between the momentum  $\mathbf{p}$  and the  $x$  axis. The superposition of Eqs. (1) and (2) of different momentum  $\mathbf{p}$  and pseudo spin  $s$  completely describes the state of Dirac fermions.

In quantum field theory, the field of SPPs is described as an operator. The quantized vector potential operator of SPPs can be obtained based on the Dyadic Green's Function approach [48] (Weyl gauge  $\hat{\mathbf{E}}(\mathbf{r}, t) + \partial\hat{\mathbf{A}}(\mathbf{r}, t)/\partial t = 0$  is used throughout this paper [49])

$$\begin{aligned} \hat{A}_i(\mathbf{r}, t) = & \sum_{j=x,y,z} \int_0^{+\infty} d\omega \int_V d^3\mathbf{r}' \sqrt{\text{Im}[\varepsilon_r(\mathbf{r}', \omega)]} \frac{\varepsilon_0 \hbar \omega^2}{\pi} \\ & \times [G_{ij}(\mathbf{r}, \mathbf{r}'; \omega) \hat{a}_j(\mathbf{r}'; \omega) e^{-i\omega t} \\ & + G_{ij}(\mathbf{r}, \mathbf{r}'; -\omega) \hat{a}_j^\dagger(\mathbf{r}'; \omega) e^{i\omega t}], \end{aligned} \quad (3)$$

where  $i = x, y, z$ ;  $G_{ij}(\mathbf{r}, \mathbf{r}'; \omega)$  are the Dyadic Green's Function of the vector potential (see Appendix A for detail);  $\hat{a}_j(\mathbf{r}'; \omega)$  and  $\hat{a}_j^\dagger(\mathbf{r}'; \omega)$  are the creation and annihilation operators of SPPs, which follow the commutation relations of bosons;  $\varepsilon_r(\mathbf{r}', \omega)$  is the permittivity in each region of the system, given as  $\varepsilon_r(\mathbf{r}, \omega) = 1 + (\varepsilon_d - 1)\Theta(-z) + i\sigma_g(\omega)/(\omega\varepsilon_0)\delta(z)$ , where  $\Theta(z)$  is the Heaviside function,  $\delta(z)$  is the Dirac function, and  $\sigma_g(\omega)$  is the conductivity of graphene, given in Refs. [1,50].

$$\begin{aligned} \sigma_g(\omega) = & \frac{ie^2 k_B T}{\pi \hbar^2 (\omega + i2\Gamma)} \left[ \frac{E_F}{k_B T} + 2 \ln(1 + e^{-E_F/k_B T}) \right] \\ & + \frac{ie^2}{4\pi \hbar} \ln \frac{2|E_F| - (\omega + i2\Gamma)\hbar}{2|E_F| + (\omega + i2\Gamma)\hbar}, \end{aligned} \quad (4)$$

where  $k_B$  is the Boltzmann constant, the temperature  $T = 300$  K, the phenomenology scattering rate  $\Gamma = 1 \times 10^{12}$  Hz, and  $E_F$  is the Fermi energy of graphene. Thus, the quantum description of SPPs is obtained.

#### B. Electron beam excitation of hot carriers

The distribution of hot carriers under the excitation of an electron beam can be calculated from the density matrix approach. Before being excited, the Dirac fermions stay in

thermal equilibrium, corresponding to a density matrix

$$\hat{\rho}_0 = \sum_{\mathbf{p}} \sum_s \sum_{\kappa} f(sv_F p) |\mathbf{p}, s, \kappa\rangle \langle \mathbf{p}, s, \kappa|, \quad (5)$$

where  $|\mathbf{p}, s, \kappa\rangle$  are the eigen states of Dirac fermions in a Dirac cone  $\kappa = K, K'$  with momentum  $\mathbf{p}$  and pseudo spin  $s$ , and  $f(E) = 1/\{1 + \exp[(E - E_F)/(k_B T)]\}$  is the Fermi-Dirac distribution.

Under the excitation of the electron beam, in the Hamiltonian of the Dirac fermions, a coupling term  $\hat{H}_{e-HC} = ev_F(\boldsymbol{\sigma} \cdot \mathbf{A}_e^K + \boldsymbol{\sigma}^* \cdot \mathbf{A}_e^{K'})$  occurs, where  $\mathbf{A}_e^K$  ( $\mathbf{A}_e^{K'}$ ) is the electron beam vector potential acting on the Dirac fermions in a Dirac cone  $K$  ( $K'$ ) (see Appendix B for the expression of  $\mathbf{A}_e^K$  and  $\mathbf{A}_e^{K'}$ ).

Then, the perturbation of the density matrix,  $\hat{\rho}_1 = \hat{\rho}(t) - \hat{\rho}_0$ , can be calculated. The distribution of hot carriers is the diagonal elements of the density matrix  $\hat{\rho}_1$ . For example, above the Fermi energy, in Dirac cones  $K$  and  $K'$ , the hot carrier distributions with momentum  $\mathbf{p}$  and pseudo spin  $s$  are (see Appendix C for detailed derivation)

$$g^K(\mathbf{p}, s) = g^{K'}(\mathbf{p}, s) = f(-sv_F \mathbf{p}_1) \times \left| \frac{\pi v_F e}{\hbar \omega} (e^{i\theta_1} - e^{-i\theta_1}) E_{e,x}(\mathbf{r}, \omega)|_{x=0, z=0} \right|^2, \quad (6)$$

where  $\mathbf{p}_1$  is the momentum of the hot carrier before absorbing a photon from the field of the electron beam,  $\theta$  ( $\theta_1$ ) is the angle between  $\mathbf{p}$  ( $\mathbf{p}_1$ ) and the  $x$  axis, and  $\omega$  is the frequency of the absorbed photon.  $\mathbf{p}_1$ ,  $\theta_1$ , and  $\omega$  can be obtained from energy-momentum conservation (see Appendix C for expressions).  $E_{e,x}(\mathbf{r}, \omega)$  is the  $x$  component of the electric field spectrum of the electron beam (see Appendix B). Thus, information on how the hot carrier is excited is obtained.

### C. Excitation of SPPs by HC QCE

The coupling Hamiltonian between the hot carriers and SPPs is  $\hat{H}_{HC-SPPs} = ev_F(\boldsymbol{\sigma} \cdot \hat{\mathbf{A}}^K + \boldsymbol{\sigma}^* \cdot \hat{\mathbf{A}}^{K'})$ , where  $\hat{\mathbf{A}}^K$  ( $\hat{\mathbf{A}}^{K'}$ ) is the vector potential of SPPs acting on the hot carriers in a Dirac cone  $K$  ( $K'$ ). Notice that  $\hat{\mathbf{A}}^K$  and  $\hat{\mathbf{A}}^{K'}$  are operators given by Eq. (3), while  $\mathbf{A}_e^K$  and  $\mathbf{A}_e^{K'}$  in  $\hat{H}_{e-HC}$  are classical fields. Thus,  $\hat{H}_{HC-SPPs}$  and  $\hat{H}_{e-HC}$  are actually quite different, although they may look similar at first glimpse.

Based on Fermi's golden rule and some properties of the Dyadic Green's Function, we can obtain: For hot carriers in a Dirac cone  $K, K'$  with momentum  $\mathbf{p}_0$  and pseudo spin  $s_0$ , the excitation rate of SPPs with frequency  $\omega$  and guide

wave number  $k$  is (see Appendix D for detailed derivation)

$$\begin{aligned} \Gamma^K(k, \omega; \mathbf{p}_0, s_0) &= \Gamma^{K'}(k, \omega; \mathbf{p}_0, s_0) \\ &= \sum_s \sum_i \frac{1}{|dk/d\theta|_{\theta_i(k)}} \frac{v_F e^2}{(2\pi\hbar)^2} P^\Theta(sv_F p - E_F) \\ &\quad \times \{ [ImF_{xx}(\mathbf{k}, \omega) - ImF_{xx}(\mathbf{k}, -\omega)] [1 + s_0 s \cos(\theta_i + \theta_0)] \\ &\quad + [ImF_{yx}(\mathbf{k}, \omega) - ImF_{yx}(\mathbf{k}, -\omega)] \\ &\quad + ImF_{xy}(\mathbf{k}, \omega) - ImF_{xy}(\mathbf{k}, -\omega) \} s s_0 \sin(\theta_i + \theta_0) \\ &\quad + [ImF_{yy}(\mathbf{k}, \omega) - ImF_{yy}(\mathbf{k}, -\omega)] [1 - s s_0 \cos(\theta_i + \theta_0)], \end{aligned} \quad (7)$$

where  $\mathbf{p}$  is the momentum of the hot carrier after SPPs excitation and  $\theta_i(k)$  are all possible angles between  $\mathbf{p}$  and the  $x$  axis. These two quantities are given by the energy-momentum conservation.  $F_{ij}(\mathbf{k}, \omega)$  are the Fourier transformation of the Dyadic Green's Function  $G_{ij}(\mathbf{r}, \mathbf{r}'; \omega)|_{z=z'=0}$  on the  $x, y$  directions. The direction of  $\mathbf{k}$  is determined by its length, given later in Eq. (8).  $\theta_0$  is the angle between  $\mathbf{p}_0$  and the  $x$  axis.

The angle between the SPPs' guide wavevector  $\mathbf{k}$  and the  $x$  axis can be obtained from energy-momentum conservation. The result is

$$\begin{aligned} \varphi &= \theta_0 \pm \arccos \left[ \frac{v_p}{v_F} + \frac{\hbar(k^2 - \omega^2/v_F^2)}{2p_0 k} \right] \\ &\approx \theta_0 \pm \arccos \frac{v_p}{v_F}. \end{aligned} \quad (8)$$

In Eq. (8),  $v_p = \omega/k$  is the phase velocity of SPPs. If  $v_p$  is viewed as the phase velocity of light in dielectric materials, then Eq. (8) gives the radiation angle of ordinary Cherenkov radiation. This is the reason why HC QCE is named as it is.

The overall excitation rate of SPPs can be obtained by summing up the excitation rates of all hot carriers. Considering that both electrons and holes can contribute to HC QCE, the excitation rate of SPPs with frequency  $\omega$  and guide wave number  $k$  is

$$\begin{aligned} \Gamma(k, \omega) &= \frac{S}{\pi^2 \hbar^2} \sum_{s_0} \int_0^{+\infty} \int_0^{2\pi} p_0 dp_0 d\theta_0 g^K(\mathbf{p}_0, s_0) \\ &\quad \times \Gamma^K(k, \omega; \mathbf{p}_0, s_0). \end{aligned} \quad (9)$$

Summing up the contribution of HC SPPs with different guide wave number  $k$  in Eq. (9), the overall excitation rate of SPPs with frequency  $\omega$ , namely  $\Gamma(\omega)$ , can be obtained as well.

Just like the excitation rate that depends on the guide wave number,  $\Gamma(k, \omega)$ , the excitation rate that depends on the direction of the guide wavevector,  $\Gamma(\varphi, \omega)$ , can also be

obtained as

$$\Gamma(\varphi, \omega) = \frac{S}{\pi^2 \hbar^2} \sum_{s_0} \int_0^{+\infty} \int_0^{2\pi} p_0 dp_0 d\theta_0 g^K(\mathbf{p}_0, s_0) \times \Gamma^K(\varphi, \omega; \mathbf{p}_0, s_0), \quad (10)$$

$$\Gamma^K(\varphi, \omega; \mathbf{p}_0, s_0) = \sum_s \sum_i \frac{\Gamma^K(\omega; \mathbf{p}_0, s_0; \theta_i(\varphi), s)}{|d\varphi/d\theta|_{\theta_i(\varphi)}}, \quad (11)$$

where  $\theta_i(\varphi)$  are all possible values of momentum angle  $\theta$  given by the parameters  $\omega$ ,  $\varphi$ ,  $\mathbf{p}_0$ ,  $s_0$ ,  $s$  and energy-momentum conservation, and  $\Gamma^K(\omega; \mathbf{p}_0, s_0; \theta, s)$  is given in Appendix D.

## IV. RESULTS AND DISCUSSIONS

### A. Hot carrier distribution

Eq. (6) indicates that:

(a) The coupling Hamiltonian  $\hat{H}_{e-HC}$  does not introduce intervalley scattering. The distributions of hot carriers in Dirac cones  $K$  and  $K'$  are equivalent.

(b) According to Eq. (6), the hot carriers are created by interband excitations. This is because the distribution of hot carriers with pseudospin  $s$  relies on the unperturbed Fermi-Dirac distribution with pseudo spin  $-s$ . This phenomenon is a unique character of electron beam excitation. It originates from the fact that the velocity of the electron beam is larger than the velocity of the Dirac fermions (see Appendix C for more details). Because of this phenomenon, almost all hot carriers are in the upper half of the Dirac cone (When  $E_F < 0$ , the distribution of hot carriers in the lower half cone is proportional to the Fermi-Dirac distribution in the upper half cone, which is almost zero. When  $E_F > 0$ , the lower half cone is under the Fermi sea, all states are occupied by Dirac fermions, and transition to there cannot occur easily.).

Thus, in order to study the hot carrier distribution, we only need to discuss the distribution of hot carriers in the upper half of the Dirac cone  $K$ ,  $g^K(\mathbf{p}, +1)$  [The distribution in the lower half of the cone  $g^K(\mathbf{p}, -1)$  is close to zero and  $g^{K'}(\mathbf{p}, s) = g^K(\mathbf{p}, s)$ .] The distributions  $g^K(\mathbf{p}, +1)$  with different Fermi energies and electron beam velocities are calculated from Eq. (6), as shown in Fig. 2.

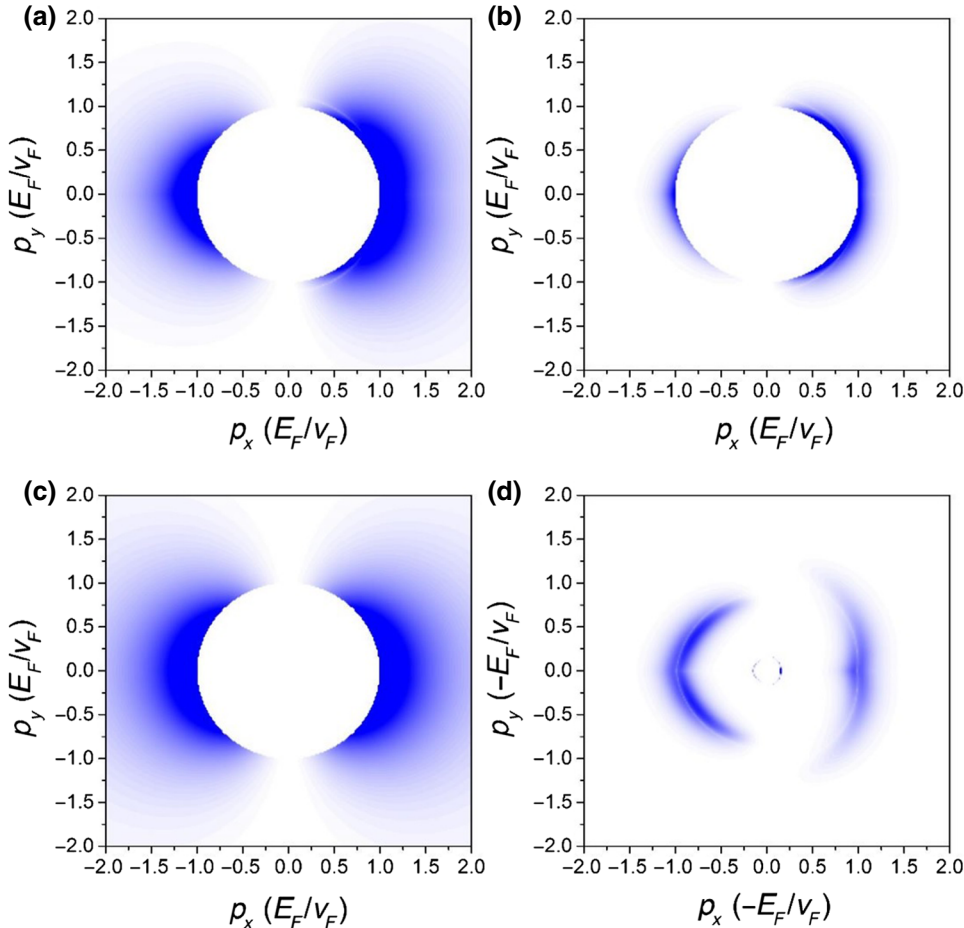


FIG. 2. Distributions of the hot carriers  $g^K(\mathbf{p}, +1)$ . The Fermi energies and electron beam velocities are: (a)  $E_F = 0.1$  eV,  $u_0 = 0.03c$ ; (b)  $E_F = 0.6$  eV,  $u_0 = 0.03c$ ; (c)  $E_F = 0.6$  eV,  $u_0 = 0.35c$ ; (d)  $E_F = -0.6$  eV,  $u_0 = 0.03c$ . In the centers of (a)–(c), there are circular areas of radius  $E_F/v_F$  without a hot carrier. These areas are the Fermi Sea, where all states are occupied by Dirac fermions.

According to Fig. 2, the hot carrier distribution is affected by the Fermi energy. When  $E_F > 0$ , the hot carriers are distributed in the  $p > E_F/v_F$  region in the momentum space due to the Fermi Sea. As the momentum becomes larger, the distribution of the hot carriers becomes sparser.

On the other hand, when  $E_F < 0$  (which means the Fermi energy is below the Dirac point), the hot carrier distribution exhibits a unique “double-ring” structure [Fig. 2(d)]. The outer ring is similar to the hot carrier distribution with Fermi energy  $|E_F|$ , while the inner ring is located near  $p = (1/9 \sim 1/8)|E_F|/v_F$  with a very narrow width on the radius direction. This peculiar inner ring originates from the near-field enhancement due to graphene SPPs’ near terahertz frequency. This inner ring does not occur when  $E_F > 0$ , because at this situation, the required photon frequency for interband hot carrier excitation is higher than the terahertz frequency.

When  $E_F = 0$ , there is no significant hot carrier excitation.

To realize the excitation of monochromatic HC SPPs, we would expect to generate a relatively simple hot carrier distribution. Therefore, in the following study, the situation where  $E_F > 0$  is discussed in detail.

According to Fig. 2, the hot carrier distribution is also affected by the electron beam velocity. The electron beam excites both the forward and backward propagating hot carriers. When the electron beam velocity is low, there are more forward propagating hot carriers; when the velocity is high, there are nearly the same number of forward and backward propagating hot carriers. At different electron velocities, the ratio between the numbers of backward and forward propagating hot carriers is shown in Fig. 3(a). The average angle  $\theta$  between  $\mathbf{p}$  and the  $x$  axis in each quadrant is shown in Fig. 3(b).

From Fig. 3, the above change rule can be explained qualitatively: Consider a Stationary Reference Frame

(SRF) where the electron beam does not move. In SRF, the near field of the electron beam forms a potential barrier on the graphene, and the Dirac fermions are incident on the potential barrier from the  $-x$  direction. When the velocity of the electron beam in the Laboratory Reference Frame (LRF) is low, the momentum of the Dirac fermions in SRF is also low. Therefore, most of the incident Dirac fermions are reflected by the potential barrier, and a relatively large reflection angle will appear. This is corresponding to the small backward-forward ratio  $N_2/N_1$  and relatively large excitation angle  $\theta$  at low electron beam velocity  $u_0$ . On the other hand, when the velocity of the electron beam in LRF is high, the momentum of the Dirac fermions in SRF is also high. Therefore, a relatively large amount of the Dirac fermions transmits through the potential barrier. The transmission and reflection angles are also relatively small. This is corresponding to the close-to-0.5 backward-forward ratio  $N_2/N_1$  and relatively small excitation angle  $\theta$  at large electron beam velocity  $u_0$ .

## B. The properties of the HC SPPs

The HC SPPs’ excitation rate from Eqs. (7) and (9) indicates that when  $E_F > 0$ , the HC SPPs are excited by intraband transitions. This is because of the  $\Theta(sv_F p - E_F)$  factor in Eq. (7), demonstrating that interband transition into the Fermi Sea cannot happen easily. However, this factor does not put a rigorous upper limit for the frequency of HC SPPs, because the momentum of the hot carrier after the excitation of HC SPPs’  $\mathbf{p}$  is smoothed out on the momentum space. When  $E_F < 0$ , both the intraband and interband transitions are allowed.

According to Eqs. (7) and (9), Fig. 4 is the frequency dependent excitation rates of HC SPPs  $\Gamma(\omega)$  when  $E_F > 0$ . Figure 5 is the guide wave number and frequency dependent excitation rates of HC SPPs  $\Gamma(k, \omega)$  when  $E_F > 0$ .

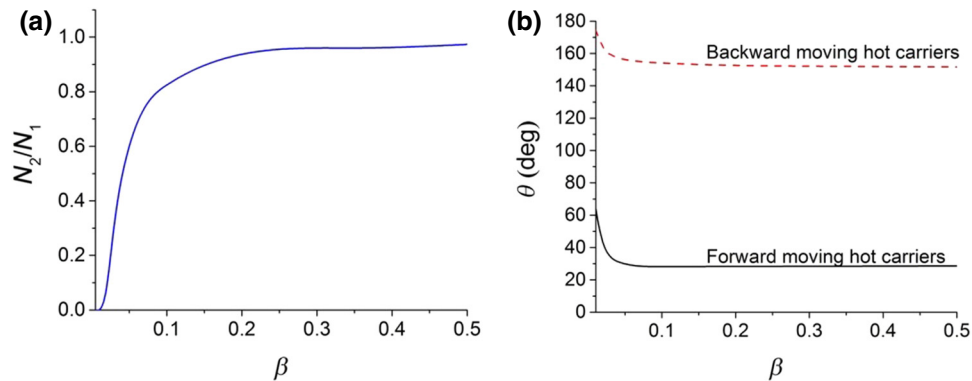


FIG. 3. (a) The ratio between the numbers of backward and forward propagating hot carriers  $N_2/N_1$  when the electron beam velocity is  $u_0 = c\beta$ . (b) The average angle  $\theta$  between  $\mathbf{p}$  and the  $x$  axis in each quadrant when the electron beam velocity is  $u_0 = c\beta$ . Because the hot carrier distribution is mirror symmetric along the  $x$  axis on momentum space, only the angles in the first and second quadrants are plotted. The Fermi energy  $E_F = 0.6$  eV.

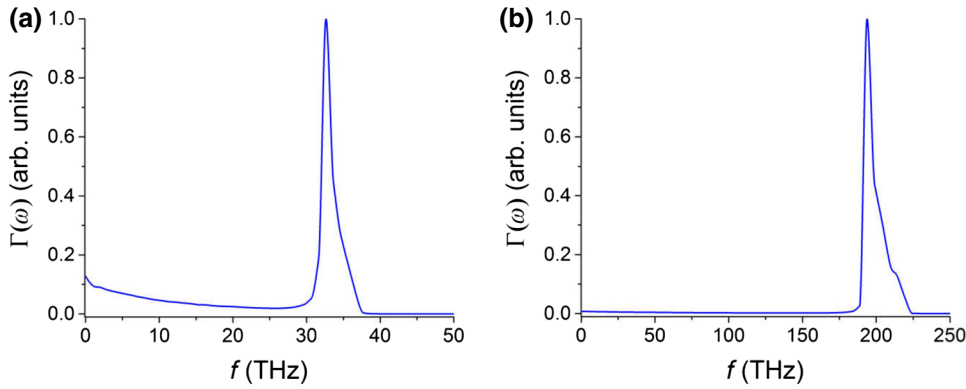


FIG. 4. The frequency dependent excitation rates of HC SPPs  $\Gamma(\omega)$ . The Fermi energies and electron beam velocities are: (a)  $E_F = 0.1$  eV,  $u_0 = 0.03c$ ; (b)  $E_F = 0.6$  eV,  $u_0 = 0.35c$ . All data are normalized by their peak values.

According to Fig. 4, the excited HC SPPs are monochromatic.

According to Fig. 5, the nonzero value of the excitation rate  $\Gamma(k, \omega)$  is concentrated at the position where the Fermi velocity  $v_F$  is slightly larger than phase velocity  $v_p$  on the SPPs' dispersion curve.

This shows that:

(a) The guide wavelength of the HC SPPs is as small as 1/300 of the vacuum wavelength and the guide wavelength bandwidth is small. Therefore, the SPPs are indeed highly confined.

(b) The values of the frequency and guide wavelength (i.e., the working point) are primarily determined by the Fermi energy of graphene. Thus, there would be great freedom to choose the electron beam velocity.

The reason for the above distribution of the excitation rate  $\Gamma(k, \omega)$  to occur is: The excitation of HC SPPs is only possible when the excitation angle  $\varphi$  is real. According to Eq. (8), this yields  $v_p < v_F$ . Therefore, HC SPPs' excitations are restricted on the right-hand side of the hot carrier dispersion curve  $\omega = v_F k$ . On the other hand, Refs. [8,9,14] show that the loss of HC SPPs grows rapidly with the guide wave number  $k$ . Thus, HC SPPs with smaller

guide wave numbers are easier to excite. Combining the two aspects, as shown in Fig. 5, the working point of HC SPPs should locate at the position where the Fermi velocity  $v_F$  is slightly larger than the phase velocity  $v_p$  on the SPPs' dispersion curve.

Further calculations based on Eqs. (7) and (9) shows that when the Fermi energy  $E_F$  grows by 1 eV, the frequency of the excited HC SPPs grows by approximately 30 THz, and the guide wave number  $k$  by  $2\pi \times 30$  THz/ $v_F$ .

According to Eqs. (7) and (9), Fig. 6 is the excitation angle and frequency dependent excitation rate  $\Gamma(\varphi, \omega)$ . The figure shows that there are four propagation directions of HC SPPs. Two of the directions are forward and the other two are backward. When the electron beam velocity  $u_0$  is low, the HC SPPs on the forward direction are stronger. When the electron beam velocity  $u_0$  is high, the strengths of forward and backward excitations are close to each other.

These propagation directions of HC SPPs are similar to that of the hot carriers (Fig. 3). This is because the excitation of HC SPPs is strongest when the phase velocity of SPPs  $v_p$  is slightly smaller than the Fermi velocity  $v_F$ . According to Eq. (8),  $\varphi \approx \theta_0$ . Therefore, the propagation direction of HC SPPs is primarily determined by the direction of motion of the hot carriers.

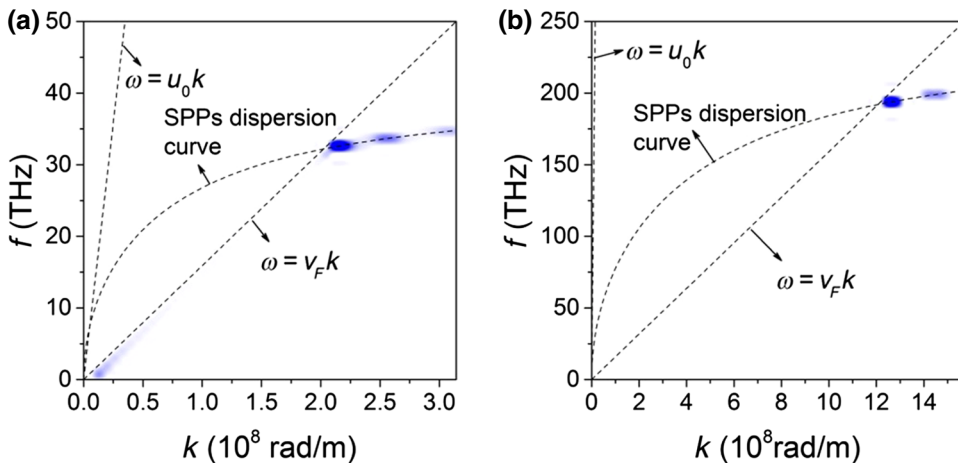


FIG. 5. The frequency and guide wave number-dependent excitation rates of HC SPPs  $\Gamma(k, \omega)$ . The Fermi energies and electron beam velocities are: (a)  $E_F = 0.1$  eV,  $u_0 = 0.03c$ ; (b)  $E_F = 0.6$  eV,  $u_0 = 0.35c$ . The dispersion curves of graphene SPPs, the electron beam ( $\omega = u_0 k$ ), and the hot carriers ( $\omega = v_F k$ ) are plotted as the dashed lines.

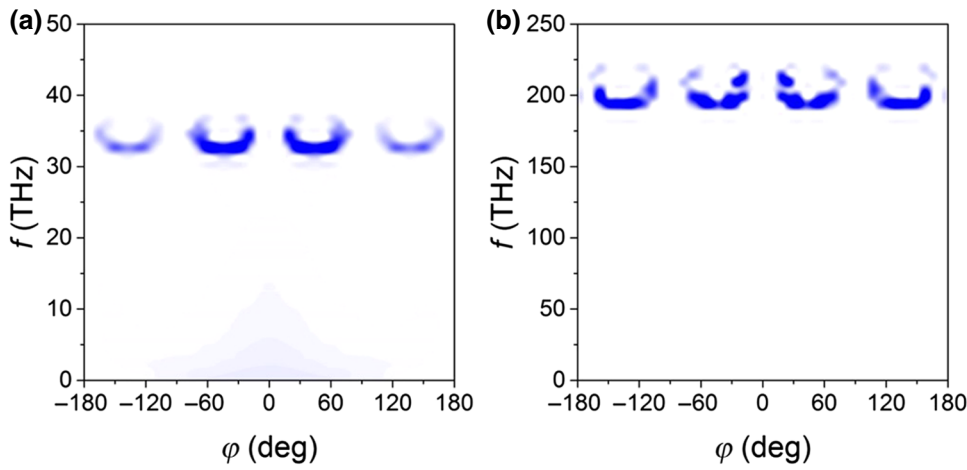


FIG. 6. The excitation angle and frequency dependent excitation rates of HC SPPs  $\Gamma(\varphi, \omega)$ . The Fermi energies and electron beam velocities are: (a)  $E_F = 0.1$  eV,  $u_0 = 0.03c$ ; (b)  $E_F = 0.6$  eV,  $u_0 = 0.35c$ .

### C. Working efficiency

The working efficiency of our method can be calculated in the following way,

First, since the excitation rate of HC SPPs  $\Gamma(\omega)$  is already known (see Sec. IV B), it is straight forward to sum it over all frequencies and obtain the total power of HC SPPs' excitation  $P_{\text{SPPs}}$ .

Second, according to Ref. [51], in our system, the total work done by the electron beam per unit time  $P_{\text{tot}}$  equals the power absorbed by graphene  $P_{\text{abs}}$ .  $P_{\text{abs}}$  can be calculated directly from the field of the electron beam  $\mathbf{E}_e(x, y, 0, t)$  and the corresponding charge current  $\mathbf{J}_e(x, y, 0, t)$  on the graphene monolayer. The first quantity  $\mathbf{E}_e(x, y, 0, t)$  can be obtained from Appendix B. The second quantity  $\mathbf{J}_e(x, y, 0, t)$  can be obtained from  $\mathbf{E}_e(x, y, 0, t)$  and the conductivity of graphene  $\sigma_g(\omega)$  in Eq. (4).

Finally, since the remaining energy of the electron beam can be collected by an electron beam collector and will not be wasted [52], the working efficiency is the ratio between  $P_{\text{SPPs}}$  and  $P_{\text{tot}}$ , namely

$$\eta = \frac{\int_0^{+\infty} \hbar\omega\Gamma(\omega)d\omega}{\iint_S \mathbf{E}_e(x, y, 0, t) \cdot \mathbf{J}_e(x, y, 0, t) dx dy}. \quad (12)$$

According to Eq. (12), at Fermi energy  $E_F = 0.6$  eV, electron beam velocity  $u_0 = 0.35c$ , and other relevant parameters, the working efficiency  $\eta$  can reach 37.28%. (It is worth noting that the working efficiency is not affected by the charge of the electron beam, because in Eq. (12), both the power of HC SPPs' excitation and the total work rely on the square of the charge  $q^2$ .)

In Sec. IV D, the x-ray emission in the system will be considered. Even at this situation, the working efficiency calculated here is still valid. This is because compared with HC SPPs' excitation, the x-ray emission due to scattering is a higher order process. Its effect on the working efficiency is relatively small.

### D. X-ray emission

In the above parts (Secs. IV A–C), we discuss the major properties of our method. In this part, we will show that when the HC SPPs and the electron beam in this method are used in the electron-plasmon scattering system [3], x-ray emission can be achieved.

In an electron-plasmon scattering system, SPPs interact with an electron beam. The result is the emission of a high-frequency photon and the change of electron beam and SPPs' momenta. Based on energy-momentum conservation, the angular frequency of the emitted photon is

$$\omega_X = \omega \frac{1 - (c/v_F)\beta \cos \varphi - (\hbar\omega/\gamma mc^2)\{[(c/v_F)^2 - 1]/2\}}{1 - \beta \cos \psi + (\hbar\omega/\gamma mc^2)[1 - (c/v_F) \cos(\psi - \varphi)]}, \quad (13)$$

where  $\omega$  is the angular frequency of SPPs,  $\varphi$  is the angle between the propagation direction of SPPs and the electron beam velocity,  $\psi$  is the angle between the emission direction of the photon and the electron beam velocity,  $m$  is the rest mass of electrons,  $\beta = u_0/c$ , and  $\gamma = 1/\sqrt{1 - \beta^2}$ .

According to Eq. (13), in the case where HC SPPs are excited by an electron beam of velocity  $u_0 = 0.35c$  on a graphene monolayer of Fermi energy  $E_F = 0.6$  eV, x-rays of frequency  $3.16 \times 10^{16}$  Hz can be emitted due to the scattering between the electron beam and the HC SPPs.

According to the relevant Refs. [3,53], the electron beam energy  $E = 35$  kV and graphene Fermi energy  $E_F = 0.6$  eV are easily achievable. Furthermore, we can significantly increase the frequency of the x-rays by increasing either the electron beam energy  $E$  or the graphene Fermi energy  $E_F$ , as shown in Fig. 7.

In addition to the frequency, the average output power of the x-rays can be estimated based on classical perturbation theory and Larmor's Formula, where the result is (see



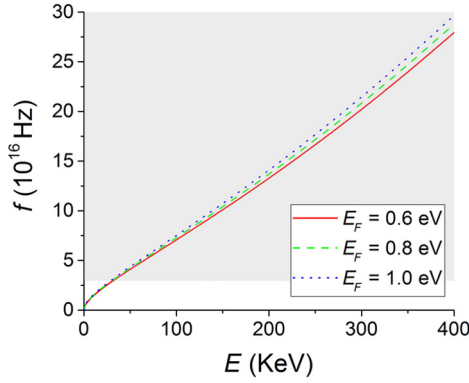


FIG. 7. The frequency of the photons emitted by electron-plasmon scattering at different electron beam energy  $E$  and graphene Fermi energy  $E_F$ . The shaded area is the x-ray frequency regime.

Appendix E for detailed derivation)

$$\begin{aligned} \bar{P} &= \int_0^{+\infty} d\omega \int_0^{2\pi} d\varphi \frac{\hbar q \gamma^2 e^3}{3\pi k \varepsilon_0^2 m^2 c^3} \\ &\times \left( 1 - \beta^2 \cos^2 \varphi + \left| \frac{\beta(\omega/c) \cos \varphi - k}{k_{z1}} \right|^2 \right) \\ &\times \frac{\Gamma(\varphi, \omega)}{(1/|k_{z1}|^2)[1/\text{Im}(k_{z1})] + (\varepsilon_s/|k_{z2}|^2)[1/\text{Im}(k_{z2})]} \\ &\times e^{-2\text{Im}k_{z1}z_0}, \end{aligned} \quad (14)$$

where  $k_{z1} = \sqrt{(\omega/c)^2 - k^2}$  and  $k_{z2} = \sqrt{\varepsilon_s(\omega/c)^2 - k^2}$ ,  $k$  is the guide wave number determined by the frequency  $\omega$  and the dispersion relation of HC SPPs.

According to Eq. (14) and the expression of  $\Gamma(\varphi, \omega)$ , Eq. (10), the radiation power  $\bar{P}$  is proportional to  $q^3$ . Therefore, it is possible to significantly increase the x-ray power by increasing the charge of the electron beam. For an electron beam with charge  $q = 1$  nC/m, the x-ray power can reach 54.14 mW, which is a considerable value for a compact system. (Other parameters are  $u_0 = 0.35c$  and  $E_F = 0.6$  eV, which are the same as those used in the discussion of x-ray frequency.)

Thus, we show that based on the scattering between HC SPPs and an electron beam, it is possible to integrate an x-ray source and the HC SPPs' emitter that drives the x-ray source in the same cavity, achieving relatively strong x-ray output with relatively low electron beam energy (35 KeV).

## V. CONCLUSION

In this paper, a method for the effective excitation of HC-SPPs that can generate x-ray radiation is presented. In the method given above, an electron beam moves along a graphene monolayer and excites hot carriers of velocity  $v_F$ .

These hot carriers are able to produce HC QCE. Here, this quantum phenomenon allows the excitation of SPPs satisfying  $v_p < v_F$ , and the excited SPPs are highly confined. Compared with traditional methods of HC SPPs' excitation [8,9,12], this method has the following advantages:

(a) In this method, no periodic structure is needed, so it is possible to achieve a miniaturized system.

(b) This method allows the excitation of monochromatic HC SPPs with a guide wavelength as small as 1/300 of the vacuum wavelength.

(c) The working point of SPPs can be dynamically tuned by the Fermi energy of graphene, but it is not sensitive to the velocity of the electron beam. This provides much more freedom in the choosing of the electron beam velocity.

(d) The working efficiency can be significantly improved. At electron beam velocity  $u_0 = 0.35c$  and graphene Fermi energy  $E_F = 0.6$  eV, the working efficiency can reach about 37.28%.

(e) When the HC SPPs and the electron beam in this method are used in the electron-plasmon scattering system, it is possible to integrate an x-ray source and the HC SPPs' emitter that drives the x-ray source in the same cavity, realizing a unified system. The electron beam energy requirement is relatively low (35 KeV).

## ACKNOWLEDGMENTS

This work is supported by the National Key Research and Development Program of China Grants No. 2018YFF01013001 and No. 2017YFA0701000, and the Natural Science Foundation of China Grants No. 61701084 and No. 61505022.

## APPENDIX A: THE DERIVATION OF THE DYADIC GREEN'S FUNCTION

According to the relation between the Dyadic Green's Function  $G_{ij}(\mathbf{r}, \mathbf{r}'; \omega)$  and vector potential  $\hat{A}_i(\mathbf{r}, t)$ , Eq. (3), the Dyadic Green's Function  $G_{ij}(\mathbf{r}, \mathbf{r}'; \omega)$  should satisfy all the boundary conditions of the vector potential  $\hat{A}_i(\mathbf{r}, t)$  at  $z = 0$  and also satisfy the following equations

$$\begin{aligned} [\nabla \times \nabla \times G(\mathbf{r}, \mathbf{r}'; \omega)]_{ij} - \frac{\omega^2}{c^2} G_{ij}(\mathbf{r}, \mathbf{r}'; \omega) \\ = \mu_0 \delta_{ij} \delta(\mathbf{r} - \mathbf{r}'), \quad z > 0, \end{aligned} \quad (A1)$$

$$\begin{aligned} [\nabla \times \nabla \times G(\mathbf{r}, \mathbf{r}'; \omega)]_{ij} - \varepsilon_d \frac{\omega^2}{c^2} G_{ij}(\mathbf{r}, \mathbf{r}'; \omega) \\ = \mu_0 \delta_{ij} \delta(\mathbf{r} - \mathbf{r}'), \quad z < 0, \end{aligned} \quad (A2)$$

where  $\delta_{ij}$  is the Kronecker delta.

Considering the situation where  $z' > 0$ , the Dyadic Green's Function can be solved by dividing it into the homogeneous part and the free space part

$$G_{ij}(\mathbf{r}, \mathbf{r}'; \omega) = \begin{cases} G_{ij}^{(0)}(\mathbf{r}, \mathbf{r}'; \omega) + G_{ij}^{(1)}(\mathbf{r}, \mathbf{r}'; \omega) & z > 0, z' > 0 \\ G_{ij}^{(0)}(\mathbf{r}, \mathbf{r}'; \omega) & z < 0, z' > 0 \end{cases}, \quad (\text{A3})$$

where the homogeneous part  $G_{ij}^{(0)}(\mathbf{r}, \mathbf{r}'; \omega)$  is the solution of the homogeneous form of Eqs. (A1) and (A2). It contains undetermined constants. The free space part  $G_{ij}^{(1)}(\mathbf{r}, \mathbf{r}'; \omega)$

is the solution of Eq. (A1) in an infinitely large space, which can be obtained by Fourier transformation without introducing undetermined constants. The undetermined constants in the homogeneous part  $G_{ij}^{(0)}(\mathbf{r}, \mathbf{r}'; \omega)$  can be obtained by substituting Eq. (A3) into the boundary conditions of the vector potential  $\hat{A}_i(\mathbf{r}, t)$  at  $z = 0$ .

When  $z' < 0$ , the Dyadic Green's Function  $G_{ij}(\mathbf{r}, \mathbf{r}'; \omega)$  can be obtained in a similar manner.

The complete expression of the Dyadic Green's Function  $G_{ij}(\mathbf{r}, \mathbf{r}'; \omega)$  is very complex. Here we only give the results that are needed for the later calculation, that is,  $G_{xx}(\mathbf{r}, \mathbf{r}'; \omega)|_{z=z'=0}$ ,  $G_{xy}(\mathbf{r}, \mathbf{r}'; \omega)|_{z=z'=0}$ ,  $G_{yx}(\mathbf{r}, \mathbf{r}'; \omega)|_{z=z'=0}$ , and  $G_{yy}(\mathbf{r}, \mathbf{r}'; \omega)|_{z=z'=0}$

$$G_{xx}(\mathbf{r}, \mathbf{r}'; \omega)|_{z=z'=0} = \frac{1}{(2\pi)^2} \iint F_{xx}(k_x, k_y, \omega) e^{i\mathbf{k}\cdot(\mathbf{r}-\mathbf{r}')} d^2\mathbf{k}, \quad (\text{A4})$$

$$G_{xy}(\mathbf{r}, \mathbf{r}'; \omega)|_{z=z'=0} = -\frac{1}{(2\pi)^2} \iint F_{yx}(k_y, -k_x, \omega) e^{i\mathbf{k}\cdot(\mathbf{r}-\mathbf{r}')} d^2\mathbf{k}, \quad (\text{A5})$$

$$G_{yx}(\mathbf{r}, \mathbf{r}'; \omega)|_{z=z'=0} = \frac{1}{(2\pi)^2} \iint F_{yx}(k_x, k_y, \omega) e^{i\mathbf{k}\cdot(\mathbf{r}-\mathbf{r}')} d^2\mathbf{k}, \quad (\text{A6})$$

$$G_{yy}(\mathbf{r}, \mathbf{r}'; \omega)|_{z=z'=0} = \frac{1}{(2\pi)^2} \iint F_{xx}(k_y, -k_x, \omega) e^{i\mathbf{k}\cdot(\mathbf{r}-\mathbf{r}')} d^2\mathbf{k}, \quad (\text{A7})$$

$F_{xx}(k_x, k_y, \omega)$

$$= \frac{(i\mu_0/2k_{z1})[1/(k_{z1}^2 + k_x^2)][2k_{z1}^2 - (c^2/\omega^2)(k_y k_x)^2 + (c^2/\omega^2)(k_{z1}^2 + k_x^2)(k_{z1}^2 + k_y^2)]}{1 + [k_{z1}/(k_{z1}^2 + k_x^2)]\{[(k_{z2}^2 + k_x^2)/k_{z2}] + \omega\mu_0\sigma_g\} - \{[(k_x k_y)^2/k_{z1}^2 + k_x^2](1 + k_{z1}/k_{z2})^2\}/\{[(1 + k_{z1}/k_{z2})k_y^2 + (1 + k_{z2}/k_{z1})k_{z1}^2 + \omega\mu_0\sigma]\}}, \quad (\text{A8})$$

$$F_{yx}(k_x, k_y, \omega) = -\frac{k_y k_x (1 + k_{z1}/k_{z2})}{(1 + k_{z1}/k_{z2})k_y^2 + (1 + k_{z2}/k_{z1})k_{z1}^2 + \omega\mu_0\sigma_g} F_{xx}(k_x, k_y, \omega), \quad (\text{A9})$$

where  $k_{z1} = \sqrt{(\omega^2/c^2) - k_x^2 - k_y^2}$  and  $k_{z2} = \sqrt{\epsilon_d(\omega^2/c^2) - k_x^2 - k_y^2}$ .

## APPENDIX B: THE ELECTROMAGNETIC FIELD OF THE ELECTRON BEAM

The electron beam in Fig. 1 is described by its equivalent charge and current density  $\rho_e(\mathbf{r}, t) = q\delta(z - z_0)\delta(x - u_0 t)$  and  $\mathbf{J}_e(\mathbf{r}, t) = \hat{\mathbf{e}}_x q u_0 \delta(z - z_0)\delta(x - u_0 t)$ , where  $q$  is the charge of the electron beam and  $\hat{\mathbf{e}}_x$  is the unit vector in the  $x$  direction. It is worth noting that the electron beam is  $y$  invariant as shown in Fig. 1.

The Fourier spectrum of the electric field  $\mathbf{E}_e(\mathbf{r}, \omega)$  excited by the electron beam satisfies the following equation

$$\nabla \times \nabla \times \mathbf{E}_e(\mathbf{r}, \omega) - \epsilon_r(\mathbf{r}, \omega) \frac{\omega^2}{c^2} \mathbf{E}_e(\mathbf{r}, \omega) = i\omega\mu_0 \mathbf{J}_e(\mathbf{r}, \omega), \quad (\text{B1})$$

where  $\mathbf{J}_e(\mathbf{r}, \omega)$  is the Fourier transformation of the current density  $\mathbf{J}_e(\mathbf{r}, t)$ . Applying the electromagnetic boundary

conditions and making use of the  $y$  invariance of the system, the expression of the electric field  $\mathbf{E}_e(\mathbf{r}, \omega)$  can be obtained. For example,  $E_{e,x}(\mathbf{r}, \omega)|_{x=0,z=0}$  that appears in Eq. (6) is

$$E_{e,x}(\mathbf{r}, \omega)|_{x=0,z=0} = \frac{-(q/2\pi)(\omega^2/k_{z1}^2 c^2)[1 - (c^2/u_0^2)]e^{ik_{z1}z_0}}{(\varepsilon_0\omega/k_{z1}) + (\varepsilon_d\varepsilon_0\omega/k_{z2}) + \sigma_g}, \quad (\text{B2})$$

where  $k_{ex} = \omega/u_0$ ,  $k_{ez1} = \sqrt{(\omega^2/c^2) - k_{ex}^2}$ , and  $k_{ez2} = \sqrt{\varepsilon_d(\omega^2/c^2) - k_{ex}^2}$

Therefore, the vector potentials  $\mathbf{A}_e^K$  and  $\mathbf{A}_e^{K'}$  satisfy

$$\begin{aligned} \mathbf{A}_e^K(\mathbf{r}, t) &= \mathbf{A}_e^{K'}(\mathbf{r}, t) = \int_{-\infty}^{+\infty} d\omega e^{-i\omega t} \frac{1}{i\omega} \mathbf{E}_e|_{z=0} \\ &= \int_{-\infty}^{+\infty} d\omega e^{-i\omega t} \frac{1}{i\omega} e^{ik_{ex}x} \left[ \mathbf{e}_x + \mathbf{e}_z \frac{k_{ex}}{k_{ez2}} \right] \\ &\quad \times E_{e,x}(\mathbf{r}, \omega)|_{x=0,z=0}. \end{aligned} \quad (\text{B3})$$

### APPENDIX C: THE DERIVATION OF THE HOT CARRIER DISTRIBUTION

Assuming under the coupling Hamiltonian  $\hat{H}_{e-\text{HC}}$ , the eigen states  $|\mathbf{p}, s, \kappa\rangle$  evolve as  $|\psi(t; \mathbf{p}, s, \kappa)\rangle$ , then the density matrix under evolution  $\hat{\rho}(t)$  is given by

$$\hat{\rho}(t) = \sum_{\mathbf{p}} \sum_s \sum_{\kappa} f(sv_F p) |\psi(t; \mathbf{p}, s, \kappa)\rangle \langle \psi(t; \mathbf{p}, s, \kappa)|. \quad (\text{C1})$$

According to the discussions in Sec. III B, the distribution of hot carriers satisfies

$$g^K(\mathbf{p}, s) = \langle \mathbf{p}, s, \kappa | \hat{\rho}(t) - \hat{\rho}_0 | \mathbf{p}, s, \kappa \rangle. \quad (\text{C2})$$

Substituting the expression of Eq. (C1) and the unperturbed density matrix  $\hat{\rho}_0$  in Sec. III B into Eq. (C2), it can be proven that

$$\begin{aligned} g^K(\mathbf{p}, s) &= \sum_{\mathbf{p}_1} \sum_{s_1} f(s_1 v_F p_1) |\langle \mathbf{p}, s, \kappa | \psi(t; \mathbf{p}_1, s_1, \kappa) \rangle|^2 \\ &\quad - f(sv_F p). \end{aligned} \quad (\text{C3})$$

Therefore, the hot carrier distribution relies on the inner product  $\langle \mathbf{p}, s, \kappa | \psi(t; \mathbf{p}_1, s_1, \kappa) \rangle$ .

Considering  $\kappa = K$ , based on the perturbation theory, the perturbed eigen states  $|\psi(t; \mathbf{p}, s, K)\rangle$  can be expressed as a summation of the unperturbed eigen states  $|\mathbf{p}, s, K\rangle$ ,

and the inner product  $\langle \mathbf{p}, s, \kappa | \psi(t; \mathbf{p}_1, s_1, \kappa) \rangle$  is obtained as

$$\begin{aligned} &\langle \mathbf{p}, s, K | \psi(t; \mathbf{p}_1, s_1, K) \rangle \\ &= \delta_{\mathbf{p}_1, \mathbf{p}} \delta_{s_1, s} - \delta_{\mathbf{p} + \hbar k_x \mathbf{e}_x - \mathbf{p}_1, 0} \frac{\pi v_F e}{\hbar \omega} (s e^{i\theta} + s_1 e^{-i\theta_1}) \\ &\quad \times E_{e,x}(\mathbf{r}, \omega)|_{x=0,z=0}, \end{aligned} \quad (\text{C4})$$

where  $\theta$  ( $\theta_1$ ) is the angle between  $\mathbf{p}$  ( $\mathbf{p}_1$ ) and the  $x$  axis,  $\omega$  is given by energy-momentum conservation  $\omega = v_F(s_1 p_1 - sp)/\hbar$ , and is the frequency of the absorbed photons in Eq. (6) in the main text. The Kronecker delta  $\delta_{\mathbf{p} + \hbar k_x \mathbf{e}_x - \mathbf{p}_1, 0}$  ensures the conservation of momentum. The momentum conservation implies that when  $\omega > 0$  and  $u_0 > v_F$ , the only possible choice of the momentum  $\mathbf{p}_1$  is

$$p_1 = \frac{1 + (v_F/u_0)^2 - 2s(v_F/u_0) \cos \theta}{1 - (v_F/u_0)^2} p, \quad (\text{C5})$$

$$\sin \theta_1 = \frac{p}{p_1} \sin \theta, \quad (\text{C6})$$

where  $s_1 = -s$ . This implies that the hot carriers are excited by interband transitions. Equations (C5) and (C6) are the expressions of momentum  $\mathbf{p}_1$  in Eq. (6) in the main text.

Substituting Eq. (C4) into Eq. (C3), and assuming that the Fermi-Dirac distribution  $f(E)$  is a small quantity when  $E > E_F$  (which is always true unless the temperature is too high), the expression of hot carrier distribution  $g^K(\mathbf{p}, s)$  is obtained as Eq. (6).

When  $\kappa = K'$ , Eq. (6) can be obtained similarly.

### APPENDIX D: THE DERIVATION OF THE SPPs' EXCITATION RATE

Let us consider a hot carrier in a Dirac cone  $\kappa = K, K'$  with momentum  $\mathbf{p}_0$  and pseudo spin  $s_0$ . Under the coupling Hamiltonian  $\hat{H}_{\text{HC-SPPs}}$ , it emits a SPP described by the Fock state  $\hat{a}_i^\dagger(\mathbf{r}; \omega)|0\rangle$  [ $\hat{a}_i^\dagger(\mathbf{r}; \omega)$  is given in Eq. (3) in the main text]. After the emission, the hot carrier momentum and pseudo spin become  $\mathbf{p}$  and  $s$ , respectively.

If  $\kappa = K$ , and according to Fermi's golden rule, the transition rate of the above-mentioned process is

$$\begin{aligned} \Gamma^K(\mathbf{p}, s; \mathbf{p}_0, s_0; n, i, \mathbf{r}, \omega) &= \frac{2\pi}{\hbar} |M(\mathbf{p}, s; \mathbf{p}_0, s_0; n, i, \mathbf{r}, \omega)|^2 \\ &\quad \times \delta(s_0 v_F p_0 - s v_F p - \hbar \omega), \end{aligned} \quad (\text{D1})$$

$$\begin{aligned} M(\mathbf{p}, s; \mathbf{p}_0, s_0; n, i, \mathbf{r}, \omega) &= \frac{v_F e}{2S} \delta_{n,1} \sqrt{\text{Im}[\varepsilon_r(\mathbf{r}, \omega)]} \frac{\varepsilon_0 \hbar \omega^2}{\pi} \\ &\quad \times \int_S d^2 \mathbf{r}'' [G_{xi}(\mathbf{r}'', \mathbf{r}; -\omega)(s_0 e^{i\theta_0} + s e^{-i\theta}) \\ &\quad + iG_{yi}(\mathbf{r}'', \mathbf{r}; -\omega)(s e^{-i\theta} - s_0 e^{i\theta_0})] e^{i((\mathbf{p}_0 - \mathbf{p}) \cdot \mathbf{r}''/\hbar)}, \end{aligned} \quad (\text{D2})$$

where  $\theta$  ( $\theta_0$ ) are the angles between  $\mathbf{p}$  ( $\mathbf{p}_0$ ) and the  $x$  axis.

Noticed that the following equation is true for the Dyadic Green's Function  $G_{ij}(\mathbf{r}, \mathbf{r}'; \omega)$

$$\begin{aligned} & \sum_{k=x,y,z} \int_V d^3\mathbf{r} \text{Im}[\varepsilon_r(\mathbf{r}, \omega)] G_{ik}(\mathbf{r}', \mathbf{r}; \omega) G_{jk}(\mathbf{r}'', \mathbf{r}; -\omega) \\ &= \frac{\mu_0 c^2}{\omega^2} \text{Im} G_{ij}(\mathbf{r}', \mathbf{r}''; \omega). \end{aligned} \quad (\text{D3})$$

Based Eq. (D3), it is possible to integrate Eq. (D1) over all possible final hot carrier states and all possible SPPs' states of certain frequency  $\omega$  (i.e., integrate over  $\mathbf{p}$ ,  $s$ ,  $n$ ,  $i$ , and  $\mathbf{r}$ ). The final SPPs excitation rate is obtained as

$$\Gamma^K(\omega; \mathbf{p}_0, s_0) = \sum_s \int_0^{2\pi} d\theta \Gamma^K(\omega; \mathbf{p}_0, s_0; \theta, s), \quad (\text{D4})$$

$$\begin{aligned} & \Gamma^K(\omega; \mathbf{p}_0, s_0; \theta, s) \\ &= \frac{v_F e^2}{(2\pi \hbar)^2 p} \sum_{\mathbf{k}} \Theta(sv_F p - E_F) \delta_{\mathbf{p}_0 - \mathbf{p} + \hbar \mathbf{k}} \\ & \times \{ \text{Im}[F_{xx}(\mathbf{k}, \omega) - F_{xx}(\mathbf{k}, -\omega)] [1 + s_0 s \cos(\theta + \theta_0)] \\ & + \text{Im}[F_{yx}(\mathbf{k}, \omega) - F_{yx}(\mathbf{k}, -\omega)] \\ & + F_{xy}(\mathbf{k}, \omega) - F_{xy}(\mathbf{k}, -\omega) ] s s_0 \sin(\theta + \theta_0) \\ & + \text{Im}[F_{yy}(\mathbf{k}, \omega) - F_{yy}(\mathbf{k}, -\omega)] [1 - s s_0 \cos(\theta + \theta_0)] \}, \end{aligned} \quad (\text{D5})$$

where  $\Theta(sv_F p - E_F)$  is the Heaviside function demonstrating that transition into the Fermi Sea cannot occur easily; the Kronecker delta  $\delta_{\mathbf{p}_0 - \mathbf{p} + \hbar \mathbf{k}}$  ensures the conservation of momentum. According to Eq. (D1), the energy conservation  $s_0 v_F p_0 - sv_F p - \hbar \omega = 0$  also holds in Eq. (D4).

Based on the energy-momentum conservation, for any fixed parameters  $\omega$ ,  $\mathbf{p}_0$ ,  $s_0$ ,  $\theta$ ,  $s$ , there is only one choice of the SPPs' guide wave number  $k = \sqrt{p_0^2 + p^2 - 2pp_0 \cos(\theta - \theta_0)}/\hbar$  [where the final momentum  $p = (s_0 v_F p_0 - \hbar \omega)/sv_F$ ]. Therefore, the integration over momentum angle  $\theta$  in Eq. (D4) can be transformed into the integration over guide wave number  $k$

$$\Gamma^K(\omega; \mathbf{p}_0, s_0) = \int_0^{+\infty} dk \Gamma^K(\omega, k; \mathbf{p}_0, s_0), \quad (\text{D6})$$

$$\Gamma^K(k, \omega; \mathbf{p}_0, s_0) = \sum_s \sum_i \frac{\Gamma^K(\omega; \mathbf{p}_0, s_0; \theta_i(k), s)}{|dk/d\theta|_{\theta_i(k)}}, \quad (\text{D7})$$

where  $\theta_i(k)$  are all possible values of momentum angle  $\theta$  given by the parameters  $\omega$ ,  $k$ ,  $\mathbf{p}_0$ ,  $s_0$ ,  $s$  and energy-momentum conservation. Substituting Eq. (D5) into Eq. (D7), Eq. (7) in the main text is obtained.

The calculation for situation  $\kappa = K'$  also gives Eq. (7).

## APPENDIX E: THE DERIVATION OF THE AVERAGE OUTPUT POWER OF X-RAYS

According to the classical theory, under the field of the HC SPPs, the motion of the electrons in the electron beam follows the equation below

$$\frac{d}{dt} \{ \gamma' [\dot{\mathbf{r}}(t)] m \dot{\mathbf{r}}(t) \} = -e \{ \mathbf{E}[\mathbf{r}(t), t] + \mu_0 \dot{\mathbf{r}}(t) \times \mathbf{H}[\mathbf{r}(t), t] \}, \quad (\text{E1})$$

where  $\mathbf{r}(t)$  is the trajectory of the electron,  $\mathbf{E}(\mathbf{r}(t), t)$  and  $\mathbf{H}(\mathbf{r}(t), t)$  are the fields of the HC SPPs on the trajectory of the electron, and  $\gamma'(\dot{\mathbf{r}}(t)) = 1/\sqrt{1 - [\dot{\mathbf{r}}(t)/c]^2}$ .

Assuming that the electrons only deviate weakly from the unperturbed trajectory  $\mathbf{r}_0(t) = u_0 t \mathbf{e}_z + y_0 \mathbf{e}_z + z_0 \mathbf{e}_z$ , Eq. (E1) is simplified as

$$\gamma^3 m \frac{d\dot{r}_{1z}(t)}{dt} = -e E_x(u_0 t, y_0, z_0, t), \quad (\text{E2})$$

$$\gamma m \frac{d\dot{r}_{1y}(t)}{dt} = -e [E_y(u_0 t, y_0, z_0, t) - \mu_0 u_0 H_z(u_0 t, y_0, z_0, t)], \quad (\text{E3})$$

$$\gamma m \frac{d\dot{r}_{1z}(t)}{dt} = -e [E_z(u_0 t, y_0, z_0, t) + \mu_0 u_0 B_y(u_0 t, y_0, z_0, t)], \quad (\text{E4})$$

where  $\gamma = \sqrt{1 - (u_0/c)^2}$  and  $\mathbf{r}_1(t) = \mathbf{r}(t) - \mathbf{r}_0(t)$ .

Then the explicit expression of the HC SPPs' electromagnetic field should be calculated. For each HC SPPs' mode with frequency  $\omega$  and direction of propagation  $\varphi$ , the longitudinal electric and magnetic fields are

$$\begin{aligned} E_x(\mathbf{r}, t; \varphi, \omega) &= \text{Re} \left[ C(\varphi, \omega) e^{i(kx \cos \varphi + ky \sin \varphi)} e^{-i\omega t} \right. \\ & \times \cos \varphi \left. \begin{cases} e^{ik_z 1z} & z > 0 \\ e^{-ik_z 2z} & z < 0 \end{cases} \right], \end{aligned} \quad (\text{E5})$$

$$\begin{aligned} H_x(\mathbf{r}, t; \varphi, \omega) &= \text{Re} \left[ C(\varphi, \omega) e^{i(kx \cos \varphi + ky \sin \varphi)} e^{-i\omega t} \right. \\ & \times \sin \varphi \left. \begin{cases} -\frac{\varepsilon_0 \omega}{k_{z1}} e^{ik_z 1z} & z > 0 \\ \frac{\varepsilon_s \varepsilon_0 \omega}{k_{z2}} e^{-ik_z 2z} & z < 0 \end{cases} \right], \end{aligned} \quad (\text{E6})$$

where  $C(\varphi, \omega)$  is the undetermined field amplitude and the guide wave number  $k$  and frequency  $\omega$  follow the

dispersion equation

$$\frac{\varepsilon_0\omega}{k_{z1}} + \frac{\varepsilon_s\varepsilon_0\omega}{k_{z2}} + \sigma_g = 0. \quad (\text{E7})$$

Based on the idea that the energy flow of each HC SPPs' mode should be consistent with the HC SPPs' excitation rate calculated by quantum theory,  $\Gamma(\varphi, \omega)$ , the field amplitude  $C(\varphi, \omega)$  is determined as (here, the imaginary part of  $k$  is ignored):

$$|C(\varphi, \omega)|^2 = \frac{8\pi(d\omega/dk)\hbar\omega\Gamma(\varphi, \omega)}{S\omega k\varepsilon_0[(1/|k'_{z1}|^2)[1/\text{Im}(k'_{z1})] + [\varepsilon_s/|k'_{z2}|^2](1/\text{Im}(k'_{z2}))]}. \quad (\text{E8})$$

Considering the fact that the HC SPPs are excited by hot carriers, it is reasonable to assume that each HC SPPs' mode is not phase related. Therefore, their effect on the electron beam can be calculated separately. Substituting Eqs. (E5) and (E6) into Eqs. (E2)–(E4), the accelerations of the electrons are obtained

$$\ddot{r}_{1x}(t; \varphi, \omega) = \text{Re} \left[ -\frac{\cos\varphi}{\gamma_0^3 m} eC(\varphi, \omega) e^{ik_y y_0} e^{ik_{z1} z_0} e^{i(k_x u_0 - \omega)t} \right], \quad (\text{E9})$$

$$\ddot{r}_{1y}(t; \varphi, \omega) = \text{Re} \left[ -\frac{\sin\varphi}{\gamma_0 m} eC(\varphi, \omega) e^{ik_y y_0} e^{ik_{z1} z_0} e^{i(k_x u_0 - \omega)t} \right], \quad (\text{E10})$$

$$\ddot{r}_{1z}(t; \varphi, \omega) = \text{Re} \left[ -\frac{\beta_0(\omega/c) \cos\varphi - k}{k_{z1} \gamma_0 m} eC(\varphi, \omega) \times e^{ik_y y_0} e^{ik_{z1} z_0} e^{i(k_x u_0 - \omega)t} \right]. \quad (\text{E11})$$

Since x-rays can penetrate graphene and the substrate freely, the radiation power of the electron is given by the famous Larmor's Formula

$$P(t; \varphi, \omega) = \frac{e^2}{6\pi\varepsilon_0 c^3} \gamma^6 \times \left\{ \ddot{\mathbf{r}}^2(t; \varphi, \omega) - \frac{1}{c^2} [\dot{\mathbf{r}}(t; \varphi, \omega) \times \ddot{\mathbf{r}}(t; \varphi, \omega)]^2 \right\}. \quad (\text{E12})$$

Using the above assumption that the electrons only deviate weakly from the unperturbed trajectory, Larmor's Formula Eq. (E12) is simplified as

$$P(t; \varphi, \omega) = \frac{e^2 \gamma^6}{6\pi\varepsilon_0 c^3} \left[ \dot{r}_{1x}^2(t; \varphi, \omega) + \frac{1}{\gamma^2} \dot{r}_{1y}^2(t; \varphi, \omega) + \frac{1}{\gamma^2} \dot{r}_{1z}^2(t; \varphi, \omega) \right]. \quad (\text{E13})$$

Substituting Eqs. (E9)–(E11) into Eq. (E13), the average radiation power from each HC SPP mode is obtained as

$$\bar{P}(\varphi, \omega) = \frac{2\hbar\gamma^2 e^4 (d\omega/dk)}{3S k \varepsilon_0^2 m^2 c^3} \left( 1 - \beta^2 \cos^2\varphi + \left| \frac{\beta_0 \frac{\omega}{c} \cos\varphi - k}{k_{z1}} \right|^2 \right) \frac{\Gamma(\varphi, \omega)}{[(1/|k_{z1}|^2)[1/\text{Im}(k_{z1})] + (\varepsilon_s/|k_{z2}|^2)[1/\text{Im}(k_{z2})]]} e^{-2\text{Im}k_{z1}z_0}. \quad (\text{E14})$$

Summing up the contribution of all modes and all electrons in the electron beam, the estimated average output power of x-rays is obtained as Eq. (13).

[1] S. Liu, C. Zhang, M. Hu, X. Chen, P. Zhang, S. Gong, T. Zhao, and R. Zhong, Coherent and tunable terahertz radiation from graphene surface plasmon polaritons excited by an electron beam, *Appl. Phys. Lett.* **104**, 201104 (2014).

[2] P. Torma and W. L. Barnes, Strong coupling between surface plasmon polaritons and emitters: A review, *Rep. Prog. Phys.* **78**, 013901 (2015).

[3] L. J. Wong, I. Kaminer, O. Ilic, J. D. Joannopoulos, and M. Soljačić, Towards graphene plasmon-based free-electron infrared to X-ray sources, *Nat. Photonics* **10**, 46 (2016).

- [4] G. Rosolen, L. J. Wong, N. Rivera, B. Maes, M. Soljačić, and I. Kaminer, Metasurface-based multi-harmonic free-electron light source, *Light-Sci. Appl.* **7**, 64 (2018).
- [5] D. E. Chang, A. S. Sørensen, P. R. Hemmer, and M. D. Lukin, Quantum Optics with Surface Plasmons, *Phys. Rev. Lett.* **97**, 053002 (2006).
- [6] M. Li, Y. Chen, G. C. Guo, and X. F. Ren, Recent progress of the application of surface plasmon polariton in quantum information processing, *Acta. Phys. Sin.* **66**, 144202 (2017).
- [7] J. Ho, J. Tatebayashi, S. Sergent, C. F. Fong, Y. Ota, S. Iwamoto, and Y. Arakawa, A Nanowire-based plasmonic quantum dot laser, *Nano Lett.* **16**, 2845 (2016).
- [8] E. D. Chubchev, I. A. Nechepurenko, A. V. Dorofeenko, A. P. Vinogradov, and A. A. Lisyansky, Highly confined surface plasmon polaritons in the ultraviolet region, *Opt. Exp.* **26**, 9050 (2018).
- [9] C. R. Williams, S. R. Andrews, S. A. Maier, A. I. Fernández-Domínguez, L. Martín-Moreno, and F. J. García-Vidal, Highly confined guiding of terahertz surface plasmon polaritons on structured metal surfaces, *Nat. Photonics* **2**, 175 (2008).
- [10] Y. Fang and M. Sun, Nanoplasmonic waveguides: Towards applications in integrated nanophotonic circuits, *Light-Sci. Appl.* **4**, e294 (2015).
- [11] C. H. Gan, H. S. Chu, and E. P. Li, Synthesis of highly confined surface plasmon modes with doped graphene sheets in the midinfrared and terahertz frequencies, *Phys. Rev. B* **85**, 125431 (2012).
- [12] V. W. Brar, M. S. Jang, M. Sherrott, J. J. Lopez, and H. A. Atwater, Highly confined tunable mid-infrared plasmonics in graphene nanoresonators, *Nano Lett.* **13**, 2541 (2013).
- [13] A. Woessner, M. B. Lundberg, Y. Gao, A. Principi, P. Alonso-González, M. Carrega, K. Watanabe, T. Taniguchi, G. Vignale, M. Polini, J. Hone, R. Hillenbrand, and F. H. L. Koppens, Highly confined low-loss plasmons in graphene–boron nitride heterostructures, *Nat. Mater.* **14**, 421 (2015).
- [14] B. Wunsch, T. Stauber, F. Sols, and F. Guinea, Dynamical polarization of graphene at finite doping, *New J. Phys.* **8**, 318 (2006).
- [15] P. A. Cherenkov, Visible emission of clean liquids by action of  $\gamma$  radiation, *Dokl. Akad. Nauk. SSSR* **2**, 451 (1934).
- [16] V. L. Ginzburg and I. M. Frank, Radiation of a uniformly moving electron due to its transition from one medium into another, *J. Phys. (USSR)* **9**, 353 (1945).
- [17] J. Alvarez-Muniz, A. Romero-Wolf, and E. Zas, Practical and accurate calculations of Askaryan radiation, *Phys. Rev. D* **84**, 103003 (2011).
- [18] J. C. Hanson and A. L. Connolly, Complex analysis of Askaryan radiation: A fully analytic treatment including the LPM effect and Cascade Form Factor, *Astropart. Phys.* **91**, 75 (2017).
- [19] G. X. Ni, A. S. McLeod, Z. Sun, L. Wang, L. Xiong, K. W. Post, S. S. Sun, B.-Y. Jiang, J. Hone, C. R. Dean, M. M. Fogler, and D. N. Basov, Fundamental limits to graphene plasmonics, *Nature* **557**, 530 (2018).
- [20] H. Lu, C. Zeng, Q. Zhang, X. Liu, M. M. Hossain, P. Reineck, and M. Gu, Graphene-based active slow surface plasmon polaritons, *Sci. Rep.* **5**, 8443 (2015).
- [21] E. H. Hwang and S. Das Sarma, Dielectric function, screening, and plasmons in two-dimensional graphene, *Phys. Rev. B* **75**, 205418 (2007).
- [22] M. Jablan, H. Buljan, and M. Soljacic, Plasmonics in graphene at infrared frequencies, *Phys. Rev. B* **80**, 245435 (2009).
- [23] K. Tantiwanichapan, J. DiMaria, S. N. Melo, and R. Paiella, Graphene electronics for terahertz electron-beam radiation, *Nanotechnology* **24**, 375205 (2013).
- [24] D. Dahal, G. Gumbs, and D. Huang, Effect of strain on plasmons, screening, and energy loss in graphene/substrate contacts, *Phys. Rev. B* **98**, 045427 (2018).
- [25] G. Gumbs and A. Balassis, Comparison of the stopping power of plasmons and single-particle excitations for nanotubes, *Phys. Rev. B* **71**, 235410 (2005).
- [26] J. Tao, L. Wu, and G. Zheng, Graphene surface-polariton in-plane Cherenkov radiation, *Carbon* **133**, 249 (2018).
- [27] S.-F. Shi, T.-T. Tang, B. Zeng, L. Ju, Q. Zhou, A. Zettl, and F. Wang, Controlling graphene ultrafast hot carrier response from metal-like to semiconductor-like by electrostatic gating, *Nano Lett.* **14**, 1578 (2014).
- [28] I. Kaminer, Y. T. Katan, H. Buljan, Y. Shen, O. Ilic, J. J. López, L. J. Wong, J. D. Joannopoulos, and M. Soljačić, Efficient plasmonic emission by the quantum Cherenkov effect from hot carriers in graphene, *Nat. Commun.* **7**, 11880 (2016).
- [29] D. K. Ferry, R. Somphonsane, H. Ramamoorthy, and J. P. Bird, Plasmon-mediated energy relaxation in graphene, *Appl. Phys. Lett.* **107**, 262103 (2015).
- [30] J. M. Hamm, A. F. Page, J. Bravo-Abad, F. J. Garcia-Vidal, and O. Hess, Nonequilibrium plasmon emission drives ultrafast carrier relaxation dynamics in photoexcited graphene, *Phys. Rev. B* **93**, 041408(R) (2016).
- [31] V. L. Ginzburg, Quantum theory of uniformly moving electrons excited light radiation in medium, *J. Exp. Theor. Phys.* **10**, 589 (1940).
- [32] J. Li, S. K. Cushing, F. Meng, T. R. Senty, A. D. Bristow, and N. Wu, Plasmon-induced resonance energy transfer for solar energy conversion, *Nat. Photonics* **9**, 601 (2015).
- [33] T. Aihara, H. Sakai, A. Takeda, S. Okahisa, M. Fukuhara, M. Ota, Y. Ishii, and M. Fukuda, Coherent plasmonic interconnection in silicon-based electrical circuit, *J. Lightwave Technol.* **33**, 2139 (2015).
- [34] L. Hu, S. Gong, M. Hu, R. Zhong, T. Zhao, and S. Liu, Enhanced dielectric waveguide mode from the coupling of surface plasmon polaritons excited by a parallel electron beam, *Opt. Commun.* **433**, 195 (2019).
- [35] A. F. Page, J. M. Hamm, and O. Hess, Polarization and plasmons in hot photoexcited graphene, *Phys. Rev. B* **97**, 045428 (2018).
- [36] L. Britnell, R. V. Gorbachev, R. Jalil, B. D. Belle, F. Schedin, A. Mishchenko, T. Georgiou, M. I. Katsnelson, L. Eaves, S. V. Morozov, N. M. R. Peres, J. Leist, A. K. Geim, K. S. Novoselov, and L. A. Ponomarenko, Field-effect tunneling transistor based on vertical graphene heterostructures, *Science* **335**, 947 (2012).
- [37] V. W. Brar, S. Wickenburg, M. Panlasigui, C.-H. Park, T. O. Wehling, Y. Zhang, R. Decker, Ç Girit, A. V. Balatsky, S. G. Louie, A. Zettl, and M. F. Crommie, Observation of Carrier-Density-Dependent Many-Body Effects in Graphene via

- Tunneling Spectroscopy, *Phys. Rev. Lett.* **104**, 036805 (2010).
- [38] M. Sanderson, Y. S. Ang, S. Gong, T. Zhao, M. Hu, R. Zhong, X. Chen, P. Zhang, C. Zhang, and S. Liu, Optical bistability induced by nonlinear surface plasmon polaritons in graphene in terahertz regime, *Appl. Phys. Lett.* **107**, 203113 (2015).
- [39] S. Gong, T. Zhao, M. Sanderson, M. Hu, R. Zhong, X. Chen, P. Zhang, C. Zhang, and S. Liu, Transformation of surface plasmon polaritons to radiation in graphene in terahertz regime, *Appl. Phys. Lett.* **106**, 223107 (2015).
- [40] H. J. Xu, W. B. Lu, W. Zhu, Z. G. Dong, and T. J. Cui, Efficient manipulation of surface plasmon polariton waves in graphene, *Appl. Phys. Lett.* **100**, 243110 (2012).
- [41] G. W. Hanson, S. A. Hassani Gangaraj, C. Lee, D. G. Angelakis, and M. Tame, Quantum plasmonic excitation in graphene and loss-insensitive propagation, *Phys. Rev. A* **92**, 013828 (2015).
- [42] A. H. Castro Neto, F. Guinea, N. M. R. Peres, K. S. Novoselov, and A. K. Geim, The electronic properties of graphene, *Rev. Mod. Phys.* **81**, 109 (2009).
- [43] C. Yu and S. Liu, Electronic-Spintronic Terahertz Emitter, *Phys. Rev. Appl.* **11**, 024055 (2019).
- [44] M. Battiato, K. Carva, and P. M. Oppeneer, Theory of laser-induced ultrafast superdiffusive spin transport in layered heterostructures, *Phys. Rev. B* **86**, 024404 (2012).
- [45] M. Amirmazlaghani and F. Raissi, Feasibility of room-temperature GHz-THz direct detection in graphene through hot-carrier effect, *IEEE Trans. Device Mater. Reliability* **18**, 429 (2018).
- [46] T. Zhao, M. Hu, R. Zhong, S. Gong, C. Zhang, and S. Liu, Cherenkov terahertz radiation from graphene surface plasmon polaritons excited by an electron beam, *Appl. Phys. Lett.* **110**, 231102 (2017).
- [47] T. Zhao, S. Gong, M. Hu, R. Zhong, D. Liu, X. Chen, P. Zhang, X. Wang, C. Zhang, P. Wu, and S. Liu, Coherent and tunable terahertz radiation from graphene surface plasmon polaritons excited by cyclotron electron beam, *Sci. Rep.* **5**, 16059 (2015).
- [48] C. Yu and S. Liu, Quantum theory of surface polariton Cherenkov light radiation source and its fluctuation, *Appl. Phys. Lett.* **114**, 181106 (2019).
- [49] R. Jackiw, Introduction to the Yang-Mills quantum theory, *Rev. Mod. Phys.* **52**, 661 (1980).
- [50] G. W. Hanson, Dyadic Green's functions and guided surface waves for a surface conductivity model of graphene, *J. Appl. Phys.* **103**, 064302 (2008).
- [51] Y. Yang, A. Massuda, C. Roques-Carnes, S. E. Kooi, T. Christensen, S. G. Johnson, J. D. Joannopoulos, O. D. Miller, I. Kaminer, and M. Soljacic, Maximal spontaneous photon emission and energy loss from free electrons, *Nat. Phys.* **14**, 894 (2018).
- [52] T. Xun, H. W. Yang, J. Zhang, and J. D. Zhang, Thermal properties of an intense relativistic electron beam collector under repetitive pulse operation, *IEEE Trans. Plasma Sci.* **44**, 957 (2016).
- [53] S. Liu, P. Zhang, W. Liu, S. Gong, R. Zhong, Y. Zhang, and M. Hu, Surface Polariton Cherenkov Light Radiation Source, *Phys. Rev. Lett.* **109**, 153902 (2012).